https://erjm.journals.ekb.eg
ISSN: 1110-1180

DOI: ---------

ERJ
Engineering Research Journal
Faculty of Engineering
Menoufia University

Modeling and Optimization of CO_2 Laser Turning Process for Armored Steel Assisted by Oxygen

Wisam.M.Farouk[1]*, Ahmed.M.Rezk[2], Wagih.W.Marzouk[2], Fayz.E.Abo Ghriba[2], El-Awady.A.Attia[3]

[1]*Mechanical Engineering department, Faculty of engineering. (Benha), Benha. University, Egypt. Email: wisam_faruk@yahoo.com, wisam.faruk@bhit.bu.edu.eg, (Corresponding author).*

[2] *Mechanical Design Department, Engineering Faculty, Minia University, Egypt.*

[3]*Industrial Engineering Department, College of engineering, Prince Sattam Bin Abdulaziz.University, Alkharj, Saudi.Arabia. & Mechanical Engineering department, Faculty of engineering (Shoubra), Benha University, Cairo, Egypt.*

Abstract:

The current paper investigates the performance of armored steel (500HB) when machined by CO_2 laser turning process (LTP) with oxygen gas assistance for grooving operation. The different working parameters were investigated which include; laser power (P), gas pressure (GP) feed rate (F) and motor speed (S). The different groove dimensions and were considered as the model responses which include; depth of cut (DC), upper cut width (UC) and lower cut width (LC), in addition to the performance aspects of root round error and metal removal rate (MRR). For this purpose, a test rig was designed and fabricated. The experimental results are mathematically modeled by response surface methodology. The results are modeled and illustrated to closely understand the effect and surface quality of CO_2-LTMP. The optimum process conditions for grooving Armored Steel (500HB) were identified. Results showed that, DC and width of cut and roundness error increase with increasing P and GP, but MRR decreases with increasing F. The motor speed has a moderate effect on the machining process of armored steel under investigation. The optimal combination of machining conditions maximized MRR, DC, LC, UC and minimized root round error to 0.0384 gm, 0.6632 mm, 0.2583 mm, 0.4684 mm and 15.7832 µm respectively. The error between optimum experimental results and the optimum predicted values for MRR, DC, LC, UC and root round error lie within 2.8%, 2.6%, 2.9%, 1% and 6.9%, respectively.

Keywords: Armored steel, Material removal rate (MRR), Response surface methodology (RSM), laser turning process (LTP).

1. Introduction

In reasons of the hardness and strong properties of most armored steel alloys, traditional machining processes provide high rate of tool wear and high cost. On the other side, nontraditional machining especially Laser machining is a recent high precision, flexible and powerful machining of hard material to process production [1][2]. In Laser machining, the turning procedure is utilized to expel the volume of material through melting and evaporation. High enthusiasm for the utilization of lasers for useful industry can be ascribed to several features that are used in wide range of applications, for example, high directionality beam, coherent, elimination of finishing operations, high product quality, reduced processing cost, versatility to computerization and minimal heat affected zone [3][4], and so on. In many industry operations like scribing, cutting, grooving, drilling and material processing one must find a set of conditions that give the optimal outcomes under specific preparing limitations [5]. During the Laser Beam Machining (LBM), molten material is expelled from the grooves that done by laser turning process across the gas jets [6][7]. The laser is without a doubt the most basic machining system's component. As a kind of light, laser possesses certain wavelike properties, but also, it can behave as if consisted of particles, named photons, which have a separate amount of energy [8]. Davima et al. [9], presented some experimental investigations on CO_2 laser cutting quality of polymers. In general, it is clear that the heat affected zone decreases with the smaller values of laser power and increase with the high values of cutting speed. Nagels[10], concentrated on the influence of sulphur content in steel on oxygen assisted CO_2 laser cutting. De-Keuster [11], alluded to the applicability for monitoring purposes of two types of sensors is indicated the microphone and the photodiode. For two types, relation between the sensor output and the cut quality is presented. Ho et al. [12], suggested temperature history for cutting of ceramics heated by a CO_2 laser is analytically. Yilbas et al. [13], presented Laser processing and thermal stress analysis for cemented carbide cutting tool. It is concluded that the titanium and tantalum carbides have significantly high values for temperature gradient and thermal stress generation accomplish under the surface. Bor-Chang Lin, and Chwan-Huei, T. have Proposed that LCD glass separation can be cut by laser with controlled fracture and also pre-bending applied to this LCD glass[14]. Optimize the CO_2 laser cutting parameters for cutting 3mm thickness of stainless steel alloy indicated in [15]. Aoud, et al. [16] presented that CO_2 laser cutting of 3 mm thick of Titanium alloy sheet grade 5 Ti-6Al-4V. The work concentrated on conducting the behavior of

cutting speed (V), laser power (Pu), and gas pressure (p) on Kerf width quality and HAZ. Also, by using the Taguchi method they analyzed and optimized the relationship between laser process output variables and cutting parameters. An integrated multi response Taguchi-neural network- robust data envelopment analysis model for CO_2 laser cutting has been investigated in detail [17]. Two quality C/Cs, kerf taper and kerf width in CO_2 laser cutting were demonstrated. An optimization model for CO_2 laser cutting of mild steel is developed in [18]. The goal was to conduct the laser cutting parameter values so as to maximize the MRR while simultaneously considering practical process constraints related to kerf width, dross formation, severance energy perpendicularity deviation and surface roughness. The results in [19] show that using lower line energy and higher frequency can significantly develop the quality of hole drilled by CO_2 laser. Laser-assisted machining is a process in which a controlled laser source is used to increase the local temperature in some parts of a workpiece which are about to be cut. Therefore, the material resistance against the cutting will be reduced and machining process will lead to smaller values of cutting forces [20]. Selection of a suitable optimal range of cutting conditions is quite necessary to obtain the high-quality cut and is important task within this domain of Investigation of optimal process conditions for pulsed Nd: laser cutting of Inconel-718 sheet [21]. RSM has been conducted to improve numerical models in terms of input cutting machining conditions for geometrical quality characteristics: bottom kerf width and top kerf width. An experimental study was studied on laser assisted turning (LAT) of SiC_p/2024Al in order to investigate the effects of input variables of LAT and conventional turning (CT) on machining performance of SiC_p/2024Al [22]. An experimental study was investigated on LAT of SiC_p/2024Al in order to conduct the behaviors of input variables of LAT and CT on machining performance of SiC_p/2024Al. The process advantages of laser processing variables were analyzed by comparing the surface roughness, residual stress and surface microstructure. To compare the costs associated with production of a valve seat made of CrNi 58/41, the runs were done in [23]. The proposed technology using laser preheating is to reduce the surface mechanical properties of the machined material, and reducing the wear of the tools. Taekyum Kim, et al. [24] conducted the experimental study on CO_2 laser-assisted micro-slot milling C/Cs of borosilicate glass, micro-channels without cracks were made using the CO_2 laser irradiation as an assisting heat source and micro-end mill. The kerf quality C/Cs containing the top kerf width, bottom kerf width, and kerf taper have been conducted as the process responses and have been detected using microscope has been demonstrated in detail [25]. The runs were made and planned using L18 orthogonal array by Taguchi method with a mixed design. In the [26], a 60 (W) continuous wave CO_2 laser cutting machine was applied for cutting the extruded samples of 3mm Polystyrene sheet. The runs were designed based on the design of experiments and statistical method. According to the later discussion, many researches on how laser control parameters affect the laser machining characteristics were presented. Intensive more comprehensive research is needed, in addition, the consideration of CO_2-LTP assisted by O_2 gas for armored steel have not been considered in the previous literature. it can be deduced that CO_2-LTP need considerable development to increase the quality of the resultant machining characteristics. The aim of this study is to increase the process efficiency by studying more comprehensive working conditions, the machining characteristics and more new materials especially for armored steel which are used in many industrial applications. Therefore, it is important to recognize the best combination of machining conditions for manufacturing this steel. Moreover, it is helpful to develop the mathematical models to represent the inter-relationships of various LTP parameters and the machining characteristics. In this work, the behavior of the metal removal rate (MRR), groove upper cut width (UC), groove lower cut width (LC), groove depth of cut (DC) and roundness error (RE) are modeled with the LTP cutting parameters, includes feed rate, power of the laser beam, motor rotating speed and the pressure of assistance gas. The RSM methodology is used for such modeling process. Moreover, the optimization of the cutting parameters is implemented for maximize MRR, DC, LC, UC and minimize the root roundness error. The identification of the optimal levels of each process condition will rely on the significance of the proposed models to fit the experimental data, thus, enabling the production engineer to define suitable working conditions which save time and money and enhances the quality of the product.

2. Experimental details

2.1 Procedure

In this study, many response factors are considered for investigating the process efficiency. These responses include: Metal Removal Rate (MRR), Roundness Error (RE), Lower Cut of the groove (LC), Upper Cut of the groove (UC) and the Depth of Cut (DC). These response variables will be investigated in function of the control and governing factors. The control factors represent the operation related factors of machining by CO_2 laser turning process. This group contains Laser power, assistance gas pressure, feed rate, and motor speed. The experiments were performed on a 4025 bystronic (Switzerland) CO_2 laser machine. Figure 1 shows the machine used with the test rig. The workpiece has a cylindrical shape from armored steel with 12 mm diameter and 50 mm length. The Armored steel's chemical composition is shown in Table 1. Armored steel is considered in reasons of its massive applications in military industries. It can be typed as a tempered high alloy steel which difficult to be cut

and machined by traditional machining methods. For each experiment, a new group of work pieces has been utilized. The fixed parameters and machining condition are also tabulated in Table 2. The choice for values of these conditions and parameters was taken through literature surveys, preliminary investigations and some reviews of experience. Acetone was used to clean the work pieces before and after each experiment. After that, it is dried and weighed using accurate digital balance with 0.1 mg resolution.

Table 1. Armored steel's chemical composition

C %	Si %	Mn %	P%	S %	Cr %	Ni%	Fe %
0.32	0.28	0.81	0.0073	0.0005	0.46	0.87	
Mo %	Al %	Co %	Cu %	V %	W %	Sn %	Rest
0.34	0.47	0.017	0.21	0.34	0.005	0.001	

Table 2. Parameters for CO_2 laser turning process

Working parameters	Description
CO_2 Laser power (W)	1000-3000
Speed (m/min)	10-40
Material thickness (mm)	1-25
Gas pressure (bar)	5-18
Lens focal length (mm)	150
Stand-off space (mm)	1
Nozzle diameter (mm)	0.8
Assistance gas type	Oxygen

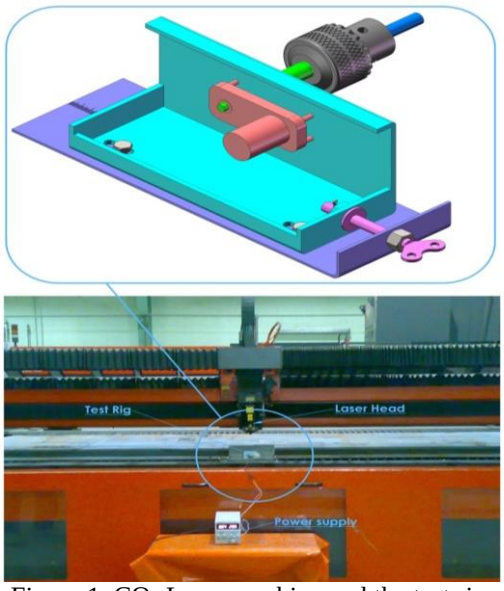

Figure 1. CO_2 Laser machine and the test rig

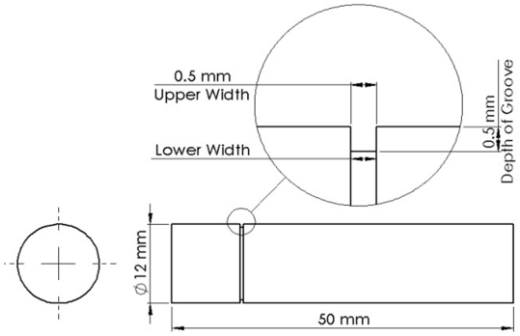

Figure 2. Geometry shape for the groove to be generated by CO_2 laser turning process

2.2 Test piece

The grooving operation is cut on a cylindrical armored steel work-piece of 12 mm diameter and 50 mm length. The geometry of specimen and the planned geometry shape for the groove to be generated by CO_2 laser turning process are shown in figure 2.

2.3 Measurements

The MRR was identified as the workpiece's weight loss after the CO_2 laser turning process (LTP) divided by the elapsed machining time. The specimens were weighted before and after machining using a precise electrical balance, as MRR=[(Wb-Wa) /t]. Considering that Wb: specimen weight before machining (g), Wa: specimen weight after machining (g), and t: observed machining time (min). The upper cut, lower cut and depth of cut were measured using Optical measuring microscope. Each value was obtained by measurements at five different places on the specimen's surface. Roundness error (RE) was measured using Roundness testing machine.

2.4 Methodology

RSM is a mixture of statistical and mathematical techniques for modeling and optimizing response variable relying on the quantitative independent variables. RSM is a successive operation, and its steps can be illustrated as shown in Fig. 3. In this investigation, the values of laser Power, (A), Gas pressure, (B), Feed rate, (C), and Motor speed, (D) setting have been determined after making some pilot trials. Table shows the values for coded and actual input process conditions. The trials are performed according to the experimental plan based on central composite rotatable second-order design (CCD). The central composite rotatable second-order design contains of 2β fractional factorial points with six center points, eight axial points, and 16 corner points

[27]. Trials matrix's Design appearing actual and coded data of the input conditions for CO_2 laser turning process are given in Table 4. The following steps were applied to the design experimental:

1- Primarily analysis was performed for identifying the effective operation range of each factor, Table 3.
2- RSM was adopted as a design of experiment.
3- According to the design of experiment, the trials were performed experientially.
4- Model responses were measured and fed to the model.
5- The optimization laser turning process parameters can be detected.

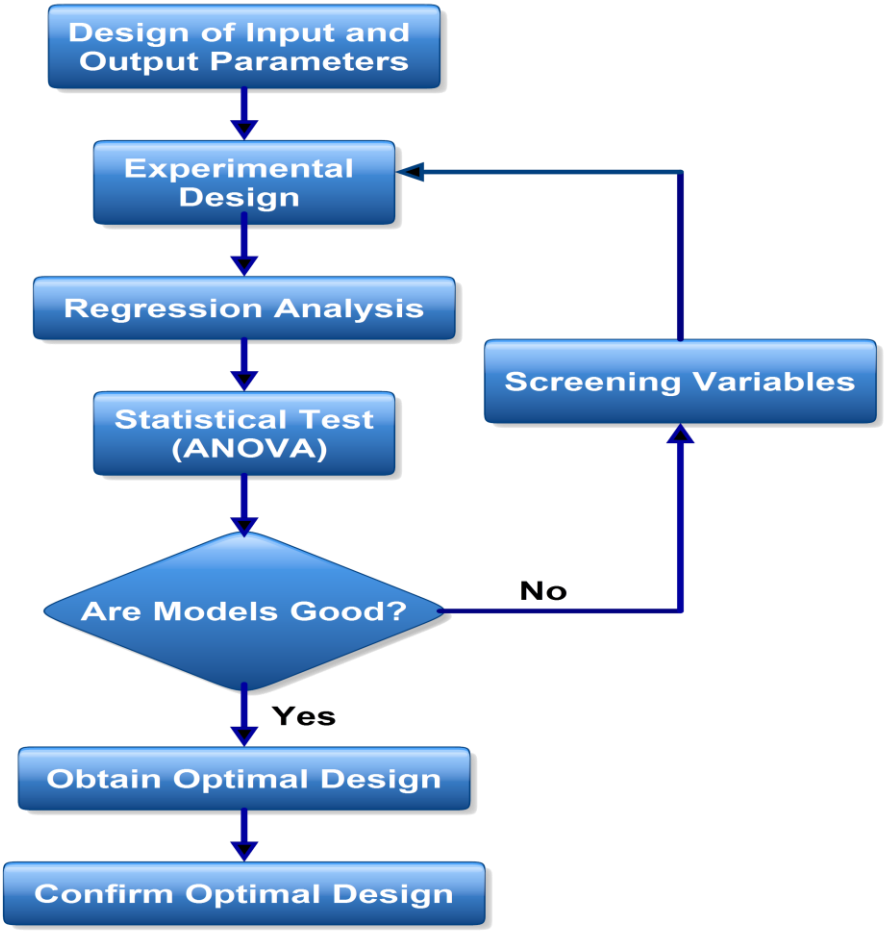

Figure 3. Procedures of the response surface methodology

Table 3: Actual and coded values of the input conditions

Input conditions	Symbols	Levels					Responses
		-2	-1	0	+1	+2	
A: Power (Watt)	X_1	1000	1500	2000	2500	3000	MRR (g/min), RE (µm), DC, UC & LC (mm)
B: O_2 gas pressure (bar)	X_2	0.2	0.3	0.4	0.5	0.6	
C: Feed rate (mm/min)	X_3	200	250	300	350	400	
D: Motor speed (r.p.m)	X_4	10	15	20	25	30	

Table 4: Design of Experiment, results, and the corresponding composite desirability

Exp. No.	Power (Watt)		Gas pressure (bar)		Feed rate (mm/min)		Motor speed (R.P.M)		Observed responses					Desirability
	Coded X_1	Actual P	Coded X_2	Actual GP	Coded X_3	Actual F	Coded X_4	Actual S	MRR g/min	RE µm	DC mm	UC mm	LC mm	
1	-1	1500	-1	0.3	-1	250	-1	15	0.034	14.407	0.338	0.391	0.220	0.382
2	1	2500	-1	0.3	-1	250	-1	15	0.03	11.039	0.793	0.389	0.253	0.575
3	-1	1500	1	0.5	-1	250	-1	15	0.032	5.952	0.376	0.473	0.200	0.392
4	1	2500	1	0.5	-1	250	-1	15	0.040	5.176	0.821	0.494	0.219	0.669
5	-1	1500	-1	0.3	1	350	-1	15	0.031	30.756	0.278	0.441	0.221	0.375
6	1	2500	-1	0.3	1	350	-1	15	0.038	55.711	0.996	0.524	0.244	0.680
7	-1	1500	1	0.5	1	350	-1	15	0.024	39.841	0.406	0.418	0.262	0
8	1	2500	1	0.5	1	350	-1	15	0.032	29.94	0.725	0.522	0.272	0.673
9	-1	1500	-1	0.3	-1	250	1	25	0.036	35.674	0.331	0.405	0.227	0.366
10	1	2500	-1	0.3	-1	250	1	25	0.032	40.972	0.690	0.388	0.278	0.482
11	-1	1500	1	0.5	-1	250	1	25	0.042	11.717	0.259	0.443	0.219	0.458
12	1	2500	1	0.5	-1	250	1	25	0.044	24.159	0.718	0.448	0.255	0.698
13	-1	1500	-1	0.3	1	350	1	25	0.042	24.236	0.289	0.354	0.208	0.142
14	1	2500	-1	0.3	1	350	1	25	0.040	19.857	0.722	0.422	0.250	0.596
15	-1	1500	1	0.5	1	350	1	25	0.032	38.722	0.517	0.387	0.231	0.302
16	1	2500	1	0.5	1	350	1	25	0.036	37.487	0.950	0.476	0.258	0.660
17	-2	1000	0	0.4	0	300	0	20	0.038	13.597	0.158	0.375	0.252	0
18	2	3000	0	0.4	0	300	0	20	0.042	12.994	1.035	0.463	0.312	0.839
19	0	2000	-2	0.2	0	300	0	20	0.038	12.842	0.687	0.449	0.254	0.570
20	0	2000	2	0.6	0	300	0	20	0.038	10.114	0.743	0.486	0.273	0.704
21	0	2000	0	0.4	-2	200	0	20	0.034	56.864	0.698	0.474	0.217	0.273
22	0	2000	0	0.4	2	400	0	20	0.026	101.542	0.759	0.453	0.210	0.192
23	0	2000	0	0.4	0	300	-2	10	0.037	7.214	0.735	0.51	0.229	0.503
24	0	2000	0	0.4	0	300	2	30	0.041	8.028	0.743	0.378	0.213	0.421
25	0	2000	0	0.4	0	300	0	20	0.042	5.342	0.839	0.4	0.23	0.517
26	0	2000	0	0.4	0	300	0	20	0.042	5.312	0.83	0.405	0.235	0.517
27	0	2000	0	0.4	0	300	0	20	0.040	5.322	0.799	0.42	0.24	0.517
28	0	2000	0	0.4	0	300	0	20	0.042	5.332	0.809	0.397	0.225	0.517
29	0	2000	0	0.4	0	300	0	20	0.041	5.342	0.839	0.4	0.23	0.517
30	0	2000	0	0.4	0	300	0	20	0.042	5.36	0.819	0.41	0.21	0.517

3. Mathematical modeling

Relying on the RSM, the regression analysis was performed. The proposed mathematical model represents the response variables in function of the independent factors as represented by equation (1).

$$Y_u = f(X_1, X_2, X_3, \ldots X_k) \pm \xi \quad (1)$$

Where the coded values of the different conditions of CO_2-LTP and responses are modeled. In other words, the u^{th} response observations are represented by Y_u and modeled in function of the corresponding (RS) represented by X_1, X_2, X_3, $X_4 \ldots X_k$ in addition to the error (ξ). In this investigation, four variables are considered (P, GP, F, and S), and a second - order polynomial regression equation, which is named quadratic equation, is adopted. The quadratic equation of Y_u can be written as equation (2) relying on the work of [27]:

$$Y_u = b_o + \sum_{i=1}^{n} b_i X_{iu} + \sum_{i=1}^{n} b_{ii} X_{iu}^2 + \sum_{j>i}^{n} b_{ij} X_{iu} X_{ju} + \varepsilon \quad (2)$$

Coefficients, b_o, b_i, b_{ij}, b_{ii} are symbols for free part, linear parts, interaction parts and quadratic parts respectively. Performing the results provided in Table 4, the form of the determined equations can be provided. The analysis of variance (ANOVA) are inspected the adequacies of the equations. The proposed mathematical model for the MRR is represented by equation (3). Based on the ANOVA results listed in Table 5, the proposed mathematical model of MRR is significant. The F-value of 13.32 indicates the equation is significant. By investigating the P-value, one can find most values ≤ 0.05 that indicate the significant of the corresponding equation terms. As shown, almost all terms are significant except the effect of the assistance gas (Oxygen) pressure, quadratic parameter of laser power (X_1^2). However, there are some insignificant interaction effect can be noticed, e.g. the interaction between P and the F, (X_1X_3), GP and the S, (X_2X_4) in addition between F and the S, (X_3X_4). The significant of the model is also noticed relying on the coefficient of determinant R^2 = 0.9255, the predicted R^2 = 0.5891 that is in sensible not agree with the adjusted R^2 = 0.8560. Examining the signal to noise ratio is also important (a ratio greater than 4 is indispensable). For MRR proposed mathematical model, the signal to noise ratio S/N = 14.542 implies a suitable signal. Relying on the ANOVA results this equation can be applied to transfer the design space. Further, the graphical diagnostics of the data are illustrated in Figure 4. In which, the predicted versus measured values are represented in figure 4.a. and the residuals are represented by figure 4.b. In residual's graph the data are scattered around the line, which demonstrate a suitable relation between predicted and experimental values. The ANOVA and the graphical diagnostics curves clearly indicate that the predictions produce by the proposed mathematical model of MRR is in suitable agree within the detected data.

$$MRR = -0.14387 + 6.04\times10^{-7}X_1 + 0.18452X_2 + 8.55\times10^{-4}X_3 + 1.721\times10^{-3}X_4 - 2.21768\times10^{-9}X_1^2 - 0.107942X_2^2 - 1.24181\times10^{-6}X_3^2 - 3.4\times10^{-5}X_4^2 + 2.9\times10^{-5}X_1X_2 + 3.3\times10^{-8}X_1X_3 - 5.45\times10^{-7}X_1X_4 - 6.15\times10^{-4}X_2X_3 + 1.325\times10^{-3}X_2X_4 + 2.052\times10^{-6}X_3X_4 \quad (3)$$

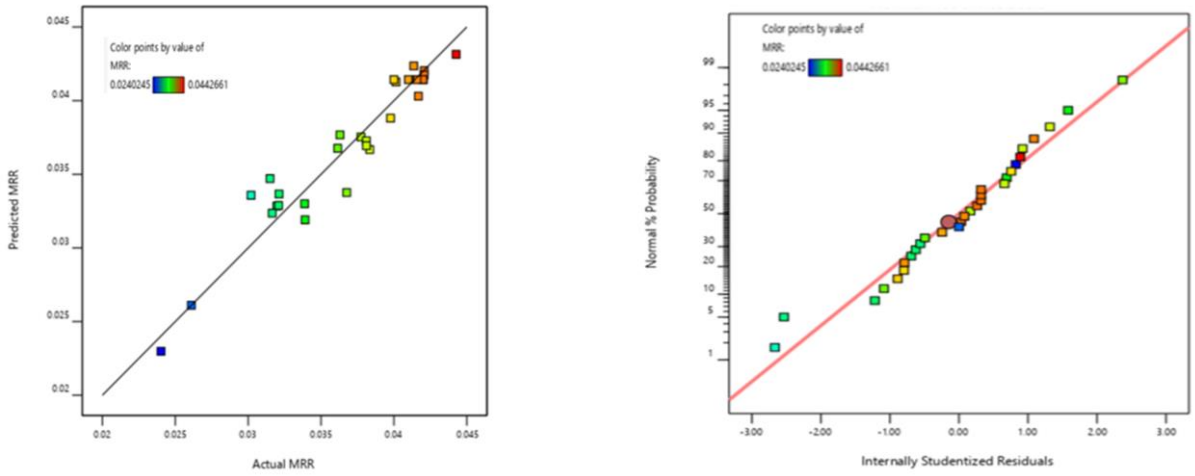

(a) Predicted vs measured va lues of MRR (b) Studentized residuals plot for MRR

Figure 4. Graphical diagnostics of the data for MRR

Table 5: ANOVA of MRR for (Armored– O_2)

Source	Sum of Squares	Degree of Freedom	Mean of Sequare	F-value	P-value	% Contribution
M	0.0007	14	0.0001	13.32	< 0.0001	12.1
X_1	0	1	0	10.02	0.0064	0
X_2	1.667E-	1	1.667E-07	0.043	0.8378	0.02
X_3	0.0001	1	0.0001	13.13	0.0025	12.1
X_4	0.0001	1	0.0001	28.87	< 0.0001	12.1
X_1^2	8.431E-	1	8.431E-06	2.19	0.1593	1.02
X_2^2	0	1	0	8.32	0.0114	0
X_3^2	0.0003	1	0.0003	68.78	< 0.0001	36.2
X_4^2	0	1	0	5.06	0.04	0
X_1X_2	0	1	0	9.06	0.0088	0
X_1X_3	0	1	0	2.83	0.113	0
X_1X_4	0	1	0	7.73	0.014	0
X_2X_3	0.0002	1	0.0002	39.36	< 0.0001	24.10
X_2X_4	7.023E-	1	7.023E-06	1.83	0.1965	0.85
X_3X_4	4.211E-	1	4.211E-06	1.10	0.3118	0.51
Residual	0.0001	15	3.843E-06			
Lack of	0.0001	10	5.442E-06	8.41	0.0149	
Pure	3.233E-	5	6.467E-07			
Cor. Total	0.0008	29				

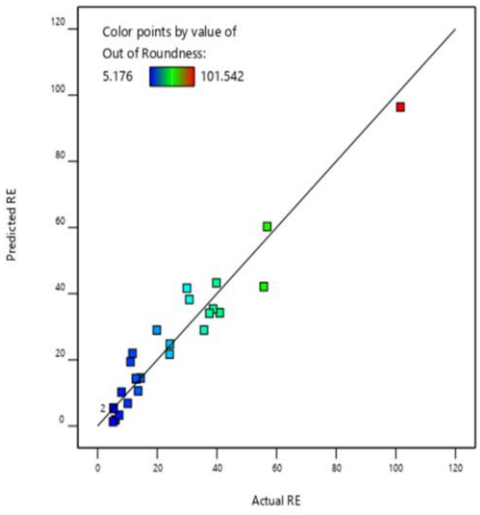

(a) Predicted vs measured values of RE

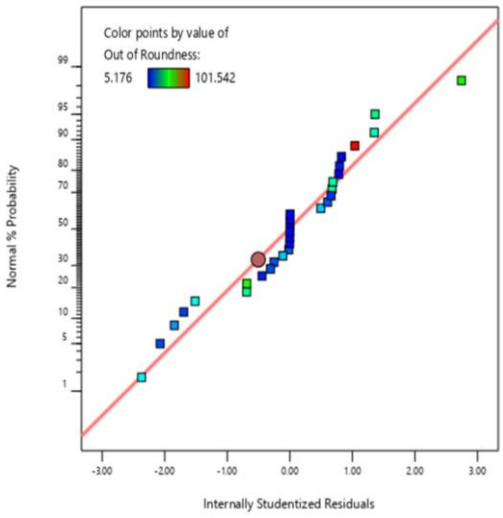

(b) Studentized residuals plot for RE

Figure 5. Graphical diagnostics of the data for RE

Table 6: ANOVA results of RE for (Armored– O_2)

Source	Sum of Squares	Degree of Freedom	Mean of Square	F-value	P-value	% Contribution
M	12604.07	14	900.29	15.34	<	6.6
X_1	19.86	1	19.86	0.338	0.569	0.15
X_2	84.80	1	84.80	1.45	0.247	0.62
X_3	1958.61	1	1958.61	33.38	<	14.4
X_4	72.21	1	72.21	1.23	0.284	0.53
X_1^2	86.32	1	86.32	1.47	0.243	0.63
X_2^2	47.77	1	47.77	0.814	0.381	0.35
X_3^2	9136.35	1	9136.35	155.7	<	67.12
X_4^2	3.46	1	3.46	0.059	0.811	0.03
X_1X_2	30.18	1	30.18	0.514	0.484	0.22
X_1X_3	1.08	1	1.08	0.018	0.893	0.01
X_1X_4	0.0924	1	0.0924	0.001	0.968	0.001
X_2X_3	310.8	1	310.80	5.3	0.036	2.28
X_2X_4	31.22	1	31.22	0.532	0.477	0.23
X_3X_4	782.52	1	782.52	13.34	0.002	5.75
Residual	880.12	15	58.67			
Lack of Fit	880.12	10	88.01	3.077	<	
Pure Error	0.0014	5	0.0003			
Cor. Total	13484.19	29				

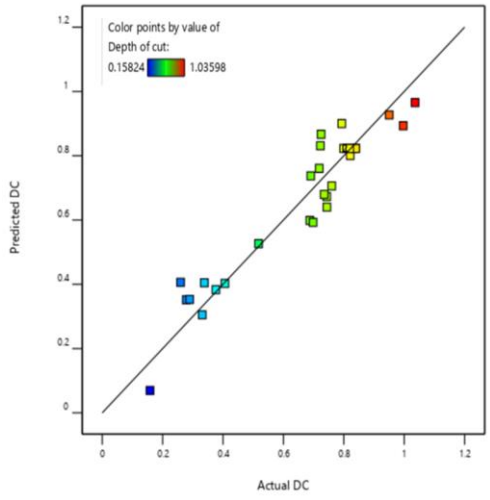

(a) Predicted vs measured values of DC

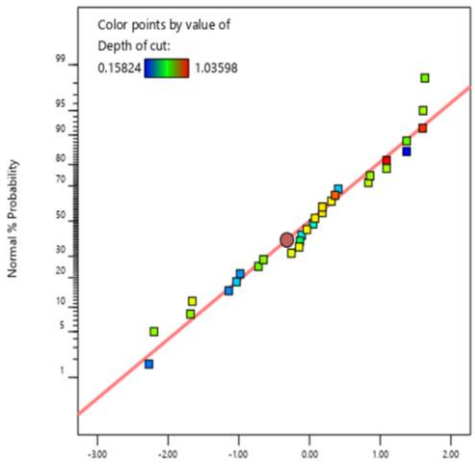

(b) Studentized residuals plot for DC

Figure 6. Graphical diagnostics of the data for DC

The mathematical model of the roundness error (RE) is presented by equation (4). The ANOVA results are shown by table 6. The obtained F-value = 15.34 indicates the equation is significant. Moreover, the obtained coefficient of determinant R^2 = 0.935, the predicted R^2 = 0.6240 is in sensible agree with the adjusted R^2 = 0.8738. The signal to noise ratio S/N =17.557 implies a suitable signal. This equation can be applied to transfer the design space. However, by examining the P-value of some terms in the equation, one can find insignificant evidence (P-value ≥ 0.10). There are three types of insignificant variables: the linear effect of P, GP and S, the interaction effect between (P×GP), (P×F), (P×S) and (GP×S) and the quadratic term of laser power (X_1^2), assistance gas (Oxygen) pressure

(X_2^2) and motor speed (X_4^2) as highlighted in table 6. Moreover, the experimental and the predicted data are illustrated by Figure 5(a) and residuals are plotted as Figure 5 (b). Results clearly demonstrate that the forecasts produced by the RE mathematical equation is in suitable agree within the measured data.

$$RE=593.58583-13.069\times10^{-3}X_1-389.75X_2-3.97X_3+6.992X_4+7.09617\times10^{-6}X_1^2+131.97X_2^2+7.3\times10^{-3}X_3^2+14.217\times10^{-3}X_4^2-27.47\times10^{-3}X_1X_2-1\times10^{-4}X_1X_3+3\times10^{-4}X_1X_4+0.881475X_2X_3+2.79375X_2X_4-0.027973X_3X_4 \quad (4)$$

For the mathematical model of the Depth of Cut (DC) provided by equation (5), the ANOVA results are listed in table 7. In which the F-value = 10.77 indicates the model is significant. The coefficient of determinant $R^2 = 0.91$, the predetermined $R^2 = 0.48$ which is in reasonable not agreement with the adjusted $R^2 = 0.83$ (the difference should be < 0.2). The signal to noise ratio S/N = 12.7 implies an adequate signal. In the other side, by investigating the P-value, one can find most values ≤ 0.05 that indicate the significant of the corresponding equation terms. As shown, almost all terms are insignificant as highlighted in table 7 except the linear effect of P, and the quadratic term of laser power (X_1^2), assistance gas (Oxygen) pressure (X_2^2), laser feed rate (X_3^2), and motor speed (X_4^2) Graphical diagnostics of the data for DC also shows satisfactory results, as shown by figure 6. The ANOVA results and graphical diagnostics of the data indicate that the proposed mathematical model is significant for DC.

$$DC=-3.21816+1.813\times10^{-3}X_1+2.3913X_2+6.583\times10^{-3}X_3+0.021156X_4-3.05364\times10^{-7}X_1^2-4.68X_2^2-17\times10^{-4}X_3^2-1.63\times10^{-3}X_4^2-389\times10^{-3}X_1X_2+4.61\times10^{-7}X_1X_3-6.32475\times10^{-6}X_1X_4+3.625\times10^{-3}X_2X_3+0.061249X_2X_4+101\times10^{-3}X_3X_4 \quad (5)$$

Table7: ANOVA of DC for (Armored – O_2)

Source	Sum of Squares	Degree of Freedom	Mean of Square	F-value	P-value	% Contribution
M	1.51	14	0.1078	10.77	< 0.0001 (significant)	6.3
X_1	1.20	1	1.20	120.3	< 0.0001	69.7
X_2	0.0083	1	0.0083	0.828	0.3772	0.48
X_3	0.0193	1	0.0193	1.93	0.1853	1.12
X_4	0.0023	1	0.0023	0.234	0.6356	0.13
X_1^2	0.1599	1	0.1599	15.97	0.0012	9.3
X_2^2	0.06	1	0.06	5.99	0.0272	3.5
X_3^2	0.0515	1	0.0515	5.15	0.0385	3
X_4^2	0.0456	1	0.0456	4.55	0.0498	2.6
X_1X_2	0.006	1	0.006	0.6039	0.4492	0.35
X_1X_3	0.0021	1	0.0021	0.211	0.6519	0.12
X_1X_4	0.004	1	0.004	0.399	0.5368	0.23
X_2X_3	0.0053	1	0.0053	0.5251	0.4798	0.31
X_2X_4	0.015	1	0.015	1.5	0.2397	0.87
X_3X_4	0.0102	1	0.0102	1.01	0.3299	0.59
Residual	0.1501	15	0.01			
Lack of Fit	0.1488	10	0.0149	55.49	0.0002	
Pure	0.0013	5	0.0003			
Cor. Total	1.66	29				

Equation (6) presents the mathematical model of the upper cut (UC). Table 8 represents the ANOVA results of the model. The obtained F-value = 9.73 that indicates the significant of the proposed equation. The statistics of the model fitting is significant, where the obtained coefficient of determinant R^2 = 0.90, predicted R^2 = 0.45 is in sensible not agree with the adjusted R^2 = 0.81. Moreover, the signal to noise ratio S/N = 11.74 that implies an appropriate signal. However, the impact of the linear effect of F, the quadratic term of laser power (X_1^2), and the interaction effect of each of (P×GP), (P×S), and (GP×S) are not significant as highlighted in table 8. Graphical diagnostics of the data for UC is illustrated by figure 7. In which, the real measurments were ploted versus the predicted values, and the studentized reseduals were ploted conter the normal percentage. Relying on these results, this proposed mathematical equation can be utilized to transfer the design space efficiently.

$$UC=1.05432-2.44\times10^{-4}X_1-0.347263X_2-2.499\times10^{-3}X_3+9.7\times10^{-5}X_4+5.73483\times10^{-9}X_1^2+1.35277X_2^2+5.01108\times10^{-6}X_3^2+3.01\times10^{-4}X_4^2+1.09\times10^{-4}X_1X_2+8.4\times10^{-7}X_1X_3-1.5248\times10^{-6}X_1X_4-2.787\times10^{-3}X_2X_3+3\times10^{-2}X_2X_4-51\times10^{-}4X_3X_4 \quad (6)$$

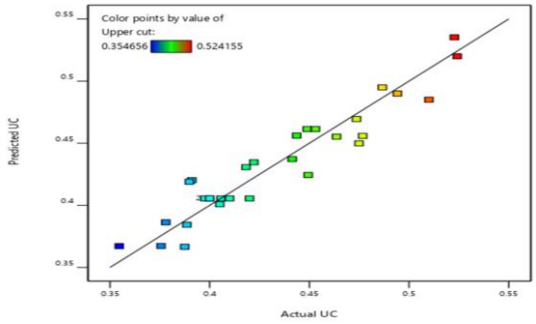

(a) Predicted vs measured values of UC

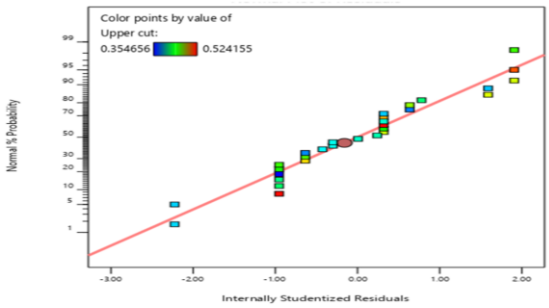

(b) Studentized residuals plot for UC

Figure 7. Graphical diagnostics of the data for UC

Table 8: ANOVA of UC for (Armored – O_2)

Source	Sum of Squares	Degree of Freedom	Mean of Sequare	F-value	P-value	% Contribution
M	0.0562	14	0.004	9.73	< 0.0001 (significant)	6.3
X_1	0.0116	1	0.0116	28.17	< 0.0001	18.3
X_2	0.0075	1	0.0075	18.08	0.0007	11.8
X_3	0.0002	1	0.0002	0.4812	0.4985	0.31
X_4	0.0146	1	0.0146	35.41	< 0.0001	22.9
X_1^2	0.0001	1	0.0001	0.1367	0.7167	0.16
X_2^2	0.005	1	0.005	12.17	0.0033	7.9
X_3^2	0.0043	1	0.0043	10.44	0.0056	6.8
X_4^2	0.0016	1	0.0016	3.77	0.0712	2.5
X_1X_2	0.0005	1	0.0005	1.15	0.3010	0.79
X_1X_3	0.0071	1	0.0071	17.11	0.0009	11.2
X_1X_4	0.0002	1	0.0002	0.5638	0.4644	0.31
X_2X_3	0.0031	1	0.0031	7.54	0.0150	4.9
X_2X_4	0	1	0	0.0873	0.7717	0
X_3X_4	0.0026	1	0.0026	6.25	0.0245	9.8
Residual	0.0062	15	0.0004			
Lack of Fit	0.0058	10	0.0006	8.27	0.0154	
Pure Error	0.0004	5	0.0001			
Cor. Total	0.0624	29				

The proposed mathematical model of the Lower Cut (LC) is presented by equation (7). Table 9 represents the ANOVA results of such model. The obtained F-value = 12.40 indicates the model is significant. The coefficient of determinant R^2 = 0.92, the predicted R^2 = 0.67 which is in sensible not agree with the adjusted R^2 = 0.85 (the difference > 0.2). The signal to noise ratio S/N= 15.22 implies adequate signal. By investigating the P-value of each term of the equation, one can find insignificant effect of some parts. The linear effects of the (GP, F and S) are not significant. The impact of the interaction effect of each of (P×GP), (P×F), (P×S) and (GP×S) are not significant. Likewise, the quadratic effect of motor speed (S) is not significant as highlighted in table 9. The Lack of Fit F-value of 0.86 implies the Lack of Fit is not significant relative to the pure error. There is a 60.82% chance that a Lack of Fit F-value this large could occur due to noise. Non-significant lack of fit is good. Supplementary, the graphical diagnostics of the data are illustrated in Figure 8. In which, the real measurments were ploted versus the predicted for LC, and the studentized reseduals were ploted conter the normal percentage. Relying on these results, the proposed mathematical equation can be utilized to transfer the design space efficiently

$$LC=0.265113-1.46\times10^{-4}X_1-1.12165X_2+1.144\times10^{-3}X_3+1.205\times10^{-2}X_4+4.92943\times10^{-8}X_1^{\,2}+0.787558X_2^{\,2}-1.89977\times10^{-6}X_3^{\,2}-1.1\times10^{-4}X_4^{\,2}-7.1\times10^{-5}X_1X_2-9.252\times10^{-8}X_1X_3+1.7748\times10^{-6}X_1X_4+2.312\times10^{-3}X_2X_3-1.876\times10^{-3}X_2X_4-3.5\times10^{-5}X_3X_4 \quad (7)$$

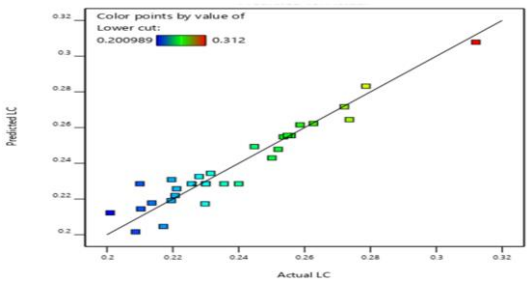

(a) Predicted vs measured values of LC

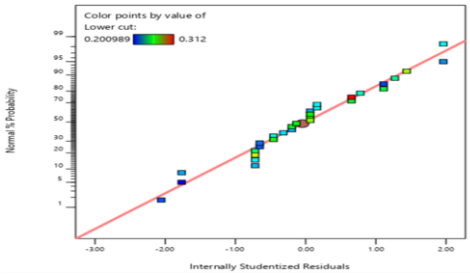

(b) Studentized residuals plot for LC

Figure 8. Graphical diagnostics of the data for LC

Table 9: ANOVA of LC for (Armored – O_2)

Source	Sum of Squares	Degree of Freedom	Mean of Sequare	F value	P value	% Contribution
M	0.0169	14	0.0012	12.4	< 0.0001 (significant)	6.78
X_1	0.0054	1	0.0054	55.41	< 0.0001	30.5
X_2	0.0001	1	0.0001	1.2	0.2905	0.56
X_3	0.0001	1	0.0001	1.49	0.2412	0.56
X_4	3.730E-	1	3.730E-07	0.0038	0.9515	0.002
X_1^2	0.0042	1	0.0042	42.75	< 0.0001	23.7
X_2^2	0.0017	1	0.0017	17.46	0.0008	9.6
X_3^2	0.0006	1	0.0006	6.35	0.0236	3.4
X_4^2	0.0002	1	0.0002	2.13	0.1653	1.13
X_1X_2	0.0002	1	0.0002	2.08	0.1694	1.13
X_1X_3	0.0001	1	0.0001	0.8784	0.3635	0.56
X_1X_4	0.0003	1	0.0003	3.23	0.0924	1.7
X_2X_3	0.0021	1	0.0021	21.95	0.0003	11.9
X_2X_4	0	1	0	0.1445	0.7092	0
X_3X_4	0.0012	1	0.0012	12.39	0.0031	6.78
Residual	0.0015	15	0.0001			
Lack of Fit	0.0009	10	0.0001	0.8617	0.6082 (not significant)	
Pure Error	0.0005	5	0.0001			
Cor. Total	0.0184	29				

4. Analysis of the parametric effect

This section presents the influences of parametric analysis for the process of CO_2 Laser turning process (LTP). The relation between the response variables and independent factors are discussed. The process responses are MRR, DC, UC, LC and RE. The input conditions include laser power (X_1 =A= P) Watt, Gas pressure (X_2=B=GP) bar, Feed rate (X_3= C=F) mm/min, and motor speed (X_4=D=S) rpm. Two dimensional response curves were drawn based on the RSM quadratic equations to check the response surface's change. The curves also provide deep understand of the relation between responses and the conditions for input process.

4.1 Material removal rate

The behavior of the MRR under different levels of the operation parameters is illustrated by figure 9. The linear variation of MRR with respect to the laser power was noticed, it can be noticed clearly using figure 9(c). Where, the effects of feed rat, and gas pressure are controlled. The nonlinear variation of MRR was noticed against the variation of feed rate, gas pressure and feet rate. Generally, the feed rate is noticed as the most contributed parameter. The effect of the feed rate depends on the level of the gas pressure. Moreover, the interaction effect of laser power and gas pressure is noticed as shown by figure 9 (a). The effect of laser power is may be caused by the heat generated by CO_2-laser. In addition, the motor speed shows a significant impact on the MRR besides the interaction effect of the gas pressure and feed rate is noticeable as shown by figure 9 (d). The MRR has a quadratic behavior under the variation of each of the gas pressure and feed rate, as shown by figure 9 (e) and (f) respectively. The increase of P means an increase in the penetration and higher energy laser beam causing more removal of the material from the groove's surface, high material removal rates are obtained at higher intensities of P and high pulse overlaps. Whereas, increase in pulse overlap increases the energy density which removes more depth of material [34, 35, 36 and 38].

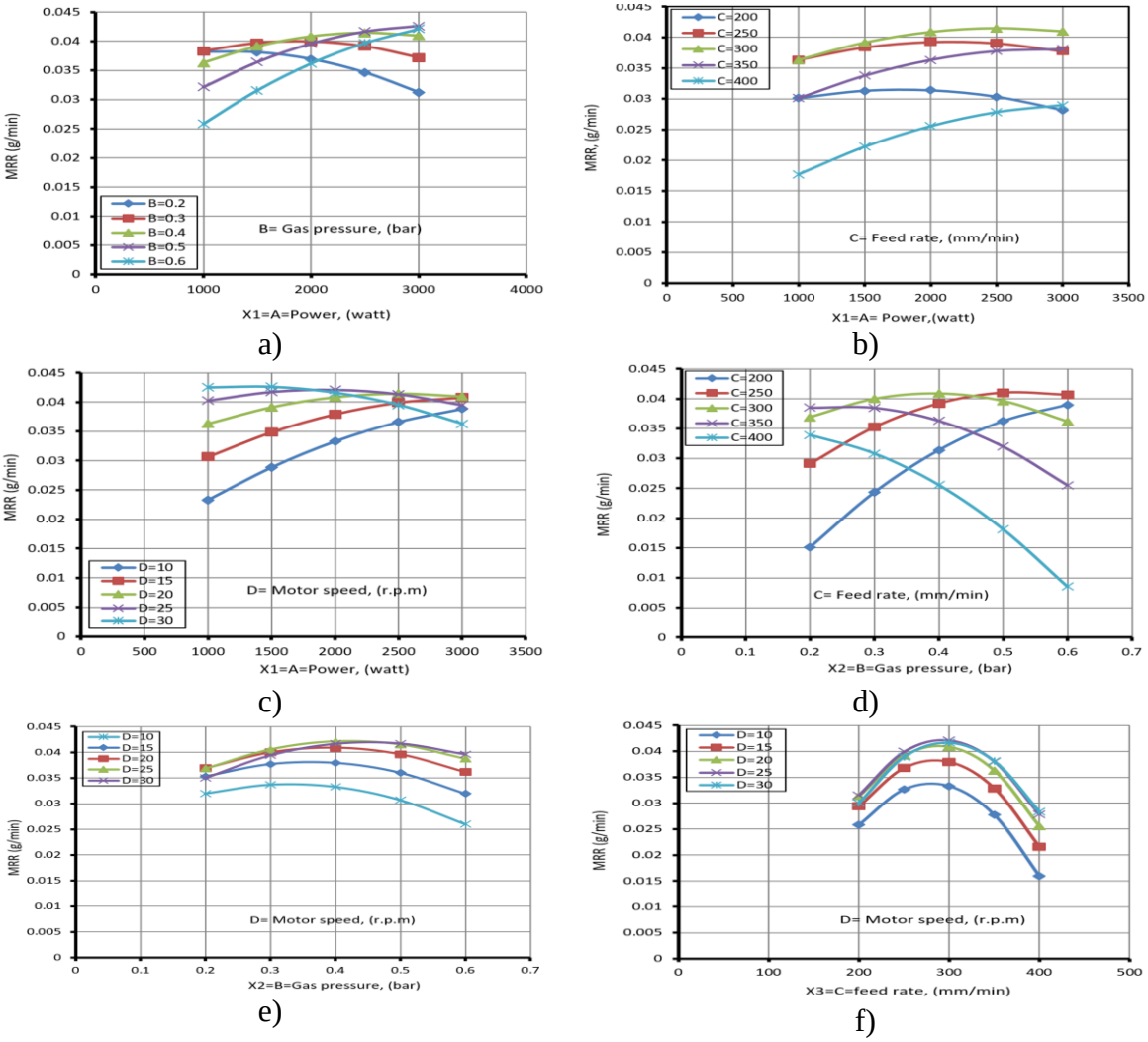

Figure 9. Effect of the process parameters on the MRR

4.2 Roundness error

Surface roundness for a machined part produced by CO_2-LTP plays an important factor in production especially for very hard materials. Surface roundness is also necessary in case of manufacturing tools and molding dies as well as drawing processes. Surface roundness of parts produced by CO_2-LTP depends on laser power, gas pressure, feed rate and motor speed. The effects of these parameters on the roundness error are represented in figure 10. As shown the, the different factors affect the roundness error. However, the most important parameter is the feed rate, this finding matched with that of [28]. The quadratic effects of feed rate, laser power, gas pressure, and motor speed are significant. The minimum error can be achieved at certain conditions. Where, the roundness error decreases with increasing variables up to specific conditions. After which, the error starts to increase as the conditions are increased and this may be attributed to the effect of cutting performance of armored steel. The interrelated effect was also noticed among different parameters e.g. feed rate and motor speed is noticed as highly significant as figure 10 (f), gas pressure with feed rate is significant as figure 10 (d).

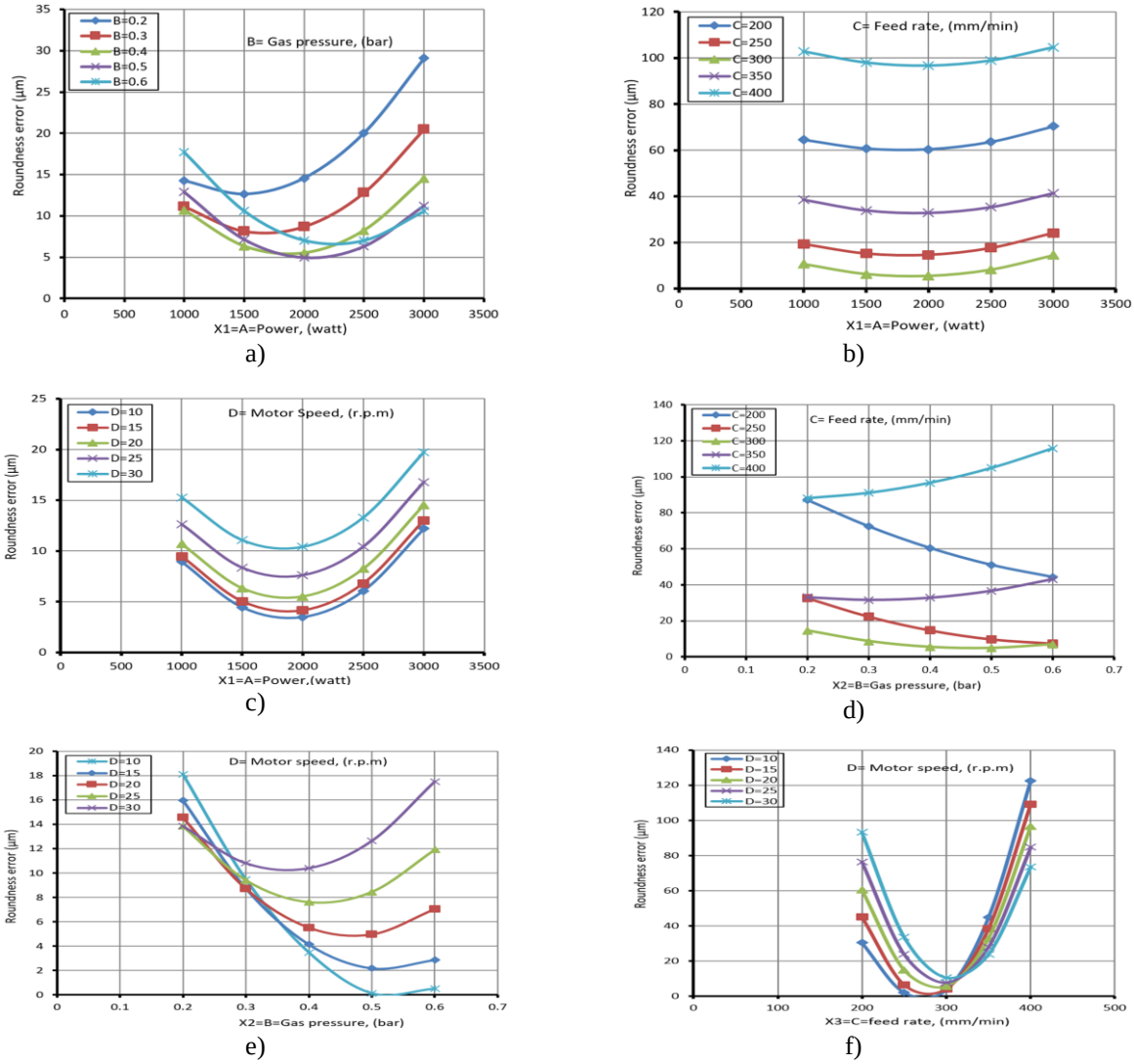

Figure 10. Behavior of roundness error at different values of operation parameters

4.3 Groove's depth of cut

The depth of cut perfumed by CO_2 laser turning processes depends on the machining parameters especially the laser power. Figure 11 illustrate the effect of the different operating parameters on the depth of cut. As shown, the depth of cut has a nonlinear relation with all parameters. Generally, the depth of cut increases as the laser power is increased and this may be explained in terms of the increased material penetration with increasing laser power [31, 32, 37 and 39]. The quadratic effect of gas pressure, feed rate, and motor speed was noticed as significant. According to these relations, the depth of cut has a maximum threshold depending on the values of this parameters.

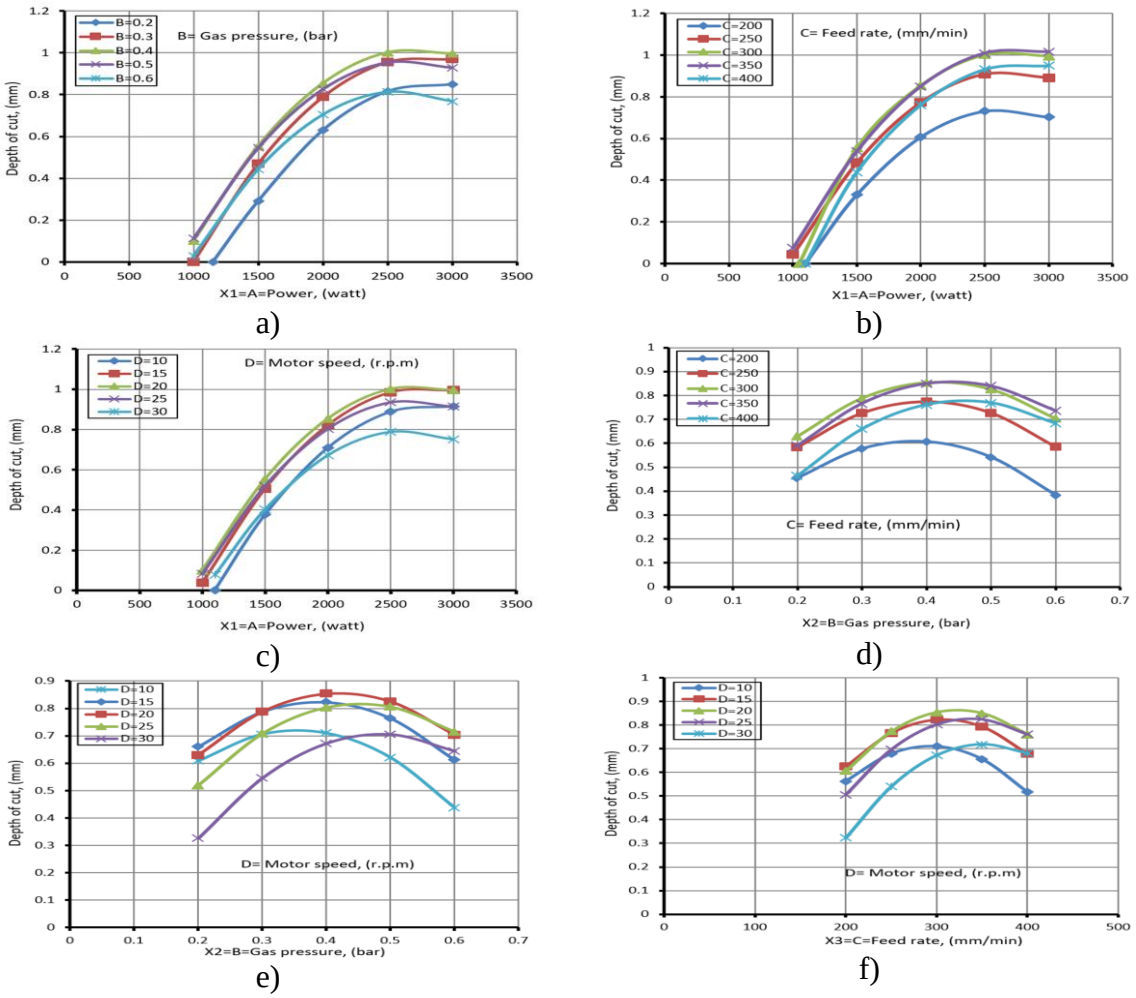

Figure 11 Behavior of the depth of groove cut under variation of operation parameters

4.4 Groove's upper cut width

Behavior of the groove's upper cut under the variation of the operation parameters is illustrated by figure 12. The nonlinear quadratic relation has been noticed with respect to all parameters. The most contributing parameter is the motor speed then comes the laser power. As the laser power increases, the upper cut is increased and this may be explained in terms of heat and energy generated during the laser process surface [31, 33]. Contrary effect was noticed for the motor speed, as the motor speed increases the upper cut reduces as shown by figure 12 (c). However, the effect of laser power is sensitive to the values of the feed rate as shown by figure 12 (b) that confirms the interaction effect of the laser power and the feed rate. The gas pressure shows a quadratic effect on the upper cut at different levels of feed rate and motor speed as shown by figure 12 (d, e). The upper cut decreases as the gas pressure is increased until certain limits after which the upper cut increases with increasing the gas pressure. Besides, there is an interrelated effect of gas pressure and motor speed on the upper cut as shown by figure 12 (e).

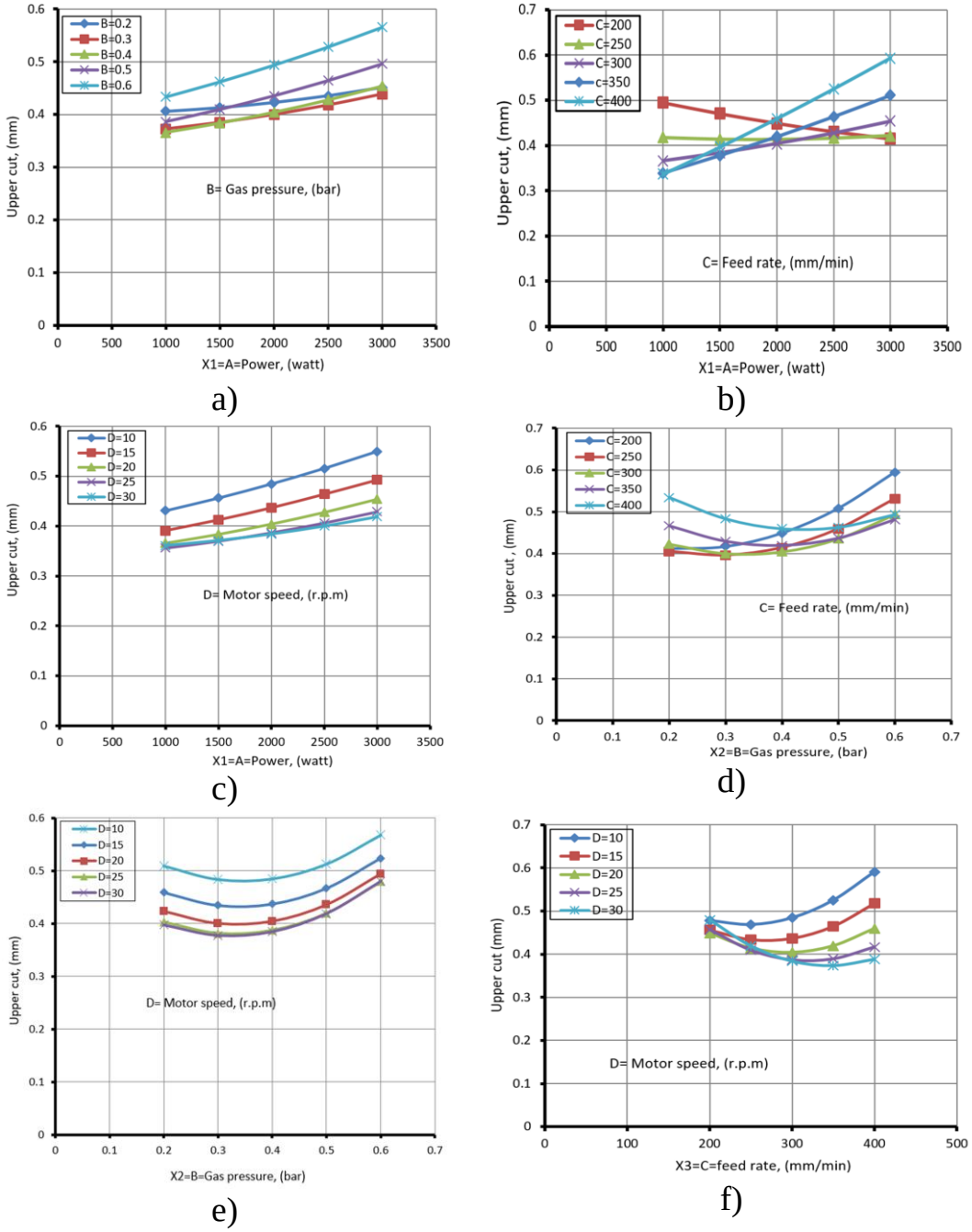

Figure.12 Behavior of the upper cut at different values of operation parameters

4.5 Groove's lower cut

During CO_2-LTMP turning operation, performing tiny lesser width is very difficult and the deviation of machined lesser width depends on the operating conditions. Figure 13 shows the behavior of the groove's lower cut width under different condition of the laser power, gas pressure, feed rate, and motor speed. The most contributing parameter is the laser power, then comes the gas pressure and the motor speed respectively. Increasing P means an increase in the energy and penetration for laser beam that increases the material removed from the machined surface [31]. The interaction effect of the gas pressure and feed rate was noticed as shown by figure 13 (d). The nonlinear quadratic relation between the lower cut and each of laser power, gas pressure, and feed rate were noticed. The interaction effect of the gas pressure and motor speed was noticed as shown in figure 13 (e).

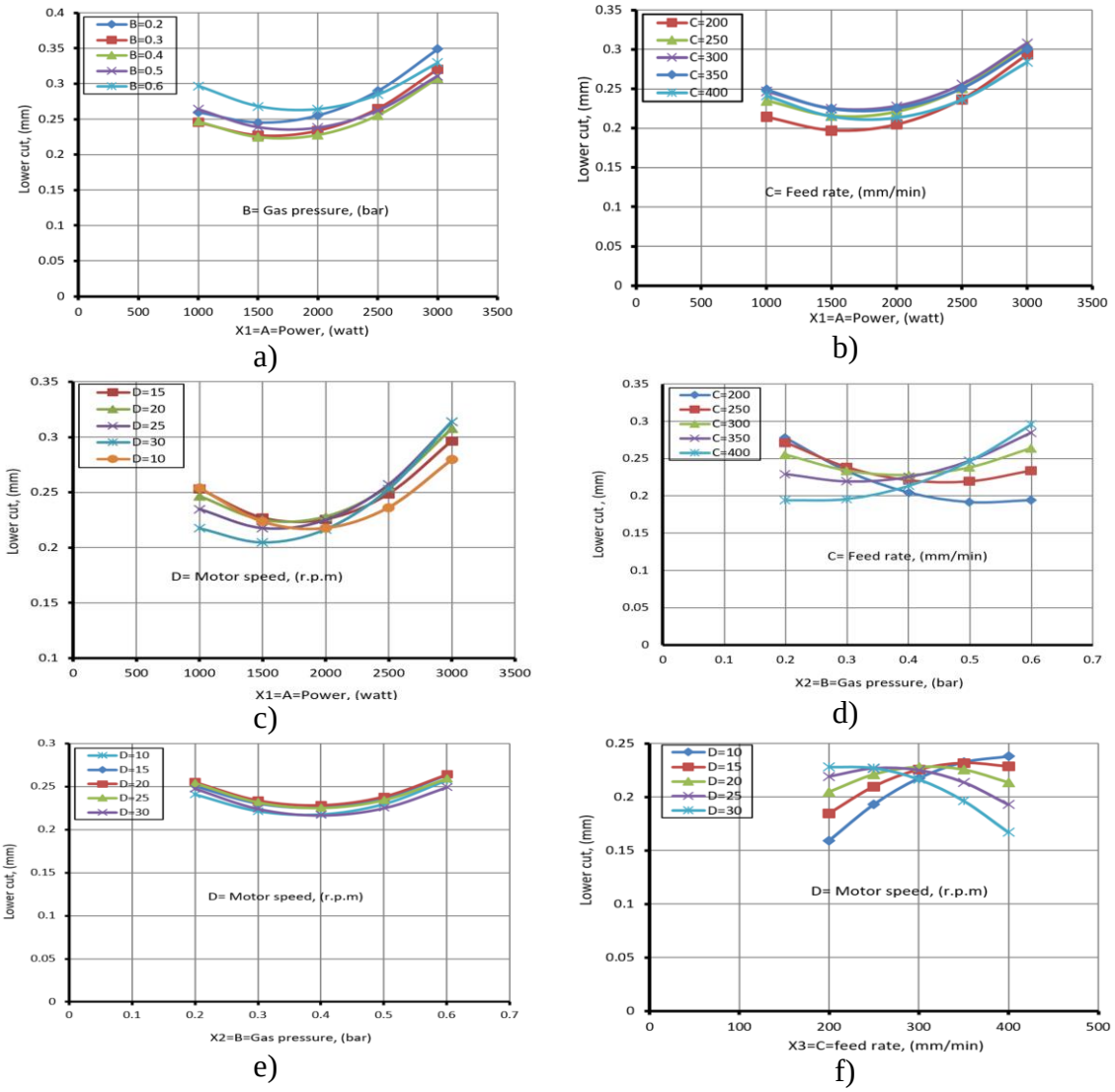

Figure. 13 Behavior of the groove lower cut at different values of the operation parameters.

5. Multi-response optimization

In this investigation, five responses have been employed, i.e. MRR, RE, DC, UC, and LC. The production objectives are to maximize MRR and the groove's dimensions (DC, UC, and LC) while minimizing the RE. A single optimal solution will not suitable for such production goal, as these objectives are conflicting in nature. Desirability is used for the multiple response optimizations. It is a modern method for industrial problems which is used to optimize multiple quality characteristics [29]. The desirability function, *D(X)* is a method which transforms an estimated response into a scale free value (*di*) called desirability and makes the use of an objective function. The range of *D(X)* was ranging from zero to one. Zero indicates that one or more responses are outside their acceptable limits; one represents the ideal case. The weighted geometric mean of the individual desirability's for the responses was called as Composite desirability. The optimal parameter conditions are considered to be the factor settings with maximum total desirability. The optimization is achieved by the simultaneous objective function which is a geometric mean of all transformed responses. The combined or composite desirability (CD) can be acquired by combining the individual desirability's [30]. Identifying the optimal input variable settings and Maximizing the composite desirability. The individual desirability is evaluated as equation (8), if it is desirable to maximize a response.

$$d_i = \begin{Bmatrix} 0 & i < L_i \\ \frac{i-L_i}{T_i-L_i} \times r_i & L_i < i < T_i \\ 1 & i > T_i \end{Bmatrix} \quad (8)$$

The individual desirability is evaluated if it is desirable to minimize a response as:

$$d_i = \begin{Bmatrix} 0 & i > H_i \\ \frac{H_i-i}{H_i-T_i} \times r_i & T_i < i < H_i \\ 1 & i < T_i \end{Bmatrix} \quad (9)$$

The individual desirability is evaluated if it is desirable to target a response as:

$$d_i = \begin{Bmatrix} \frac{i-L_i}{T_i-L_i} \times r_i & L_i < i < T_i \\ \frac{H_i-i}{H_i-T_i} \times r_i & T_i < i < H_i \\ 0 & H_i < i < L_i \end{Bmatrix} \quad (10)$$

Where; i = the expected value of i^{th} response, T_i = goal value for i^{th} response, L_i= lesser suitable value for i^{th} response, H_i = largest suitable value for i^{th} response, *di* = *D(X)* for i^{th} response, *CD* = composite desirability, r_i = desirability function's weight of the i^{th} response, w_i = the i^{th} response's importance and $W = \Sigma w_i$.

If, the composite desirability is evaluated when the importance is the same for each response as: CD $= [\prod {d_i}^{w_i}]^{\frac{1}{W}}$, but for equal importance CD$= [d_1 \times d_2 \times \dots d_n]^{\frac{1}{n}}$ (11)

Where n = number of responses. To reveal the possible difference in the importance of various responses, the weight w_i fulfils $0<w_i<1$ and $w_1+ w_2+ w_3+ \dots\dots+ w_n= 1$

The five responses (MRR, RE, DC, UC and LC) are optimized simultaneously using the composite desirability optimization technique illustrated by equations 8 to 11. The input conditions of the multi-response optimization are shown by Table 10. The composite desirability values of the 30 conducted runs are illustrated in Table 4. The optimal results are shown in figure 14 and table 11. Where figure 14 shows the optimized curves of the different responses and the optimal combination of the input operating conditions.

Table.10: Input conditions and responses limitations

Name	objective	Li	Hi	Lower W	Upper W	Importance
Power, (watt)	Is in range	1000	3000	1	1	1
Gas pressure, (bar)	Is in range	0.2	0.6	1	1	1
Feed rate, (mm/min)	Is in range	200	400	1	1	1
Motor speed, (r.p.m)	Is in range	10	30	1	1	1
MRR, (mm/min)	Max	0.0240245	0.0442661	1	1	1
RE, (μm)	Min	5.176	101.542	1	1	1
DC, (mm)	Max	0.15824	1.03598	1	1	1
UC, (mm)	Max	0.354656	0.524155	1	1	1
LC, (mm)	Max	0.200989	0.312	1	1	1

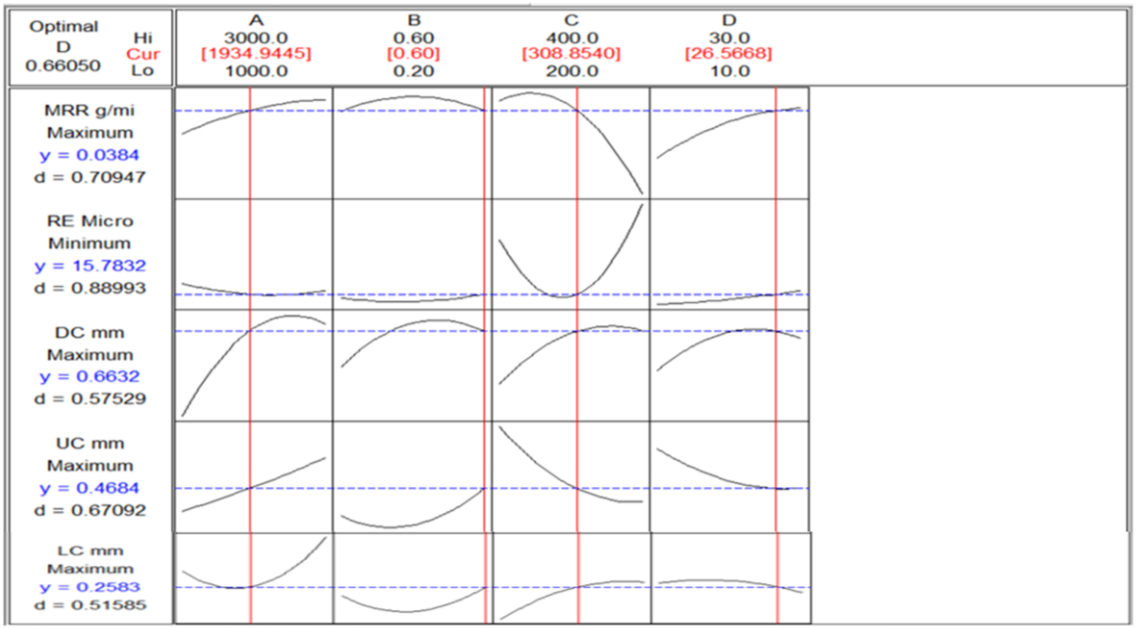

Figure. 14 Results of the multi-objective optimization of the five responses

Table 11: Optimum parameters and the corresponding expected responses

Parameter	Investigated range	Optimum value	Expected optimum responses		
			Response	Objective	Expected value
Laser Power, (Watt)	1000 – 3000	1934.944	MRR, (g/min)	Maximize	0.0384
Assistance gas pressure, (bar)	0.2 – 0.6	0.60	RE, (µm)	Minimize	15.7832
Feed rate, (mm/min)	200 – 400	308.85	DC, (mm)	Maximize	0.6632
Motor Speed, (r.p.m)	10 – 30	26.566	UC, (mm)	Maximize	0.4684
			LC, (mm)	Maximize	0.2583

Table 12: Comparison between optimal predicted and real responses.

Response	**Expected optimum responses**	**Trialing responses**	**Error (%)**
MRR , (g/min)	0.0384	0.0395	2.8
RE, (µm)	15.7832	16.205	2.6
DC , (mm)	0.6632	0.6832	2.9
UC , (mm)	0.4684	0.4732	1
LC , (mm)	0.2583	0.2777	6.9

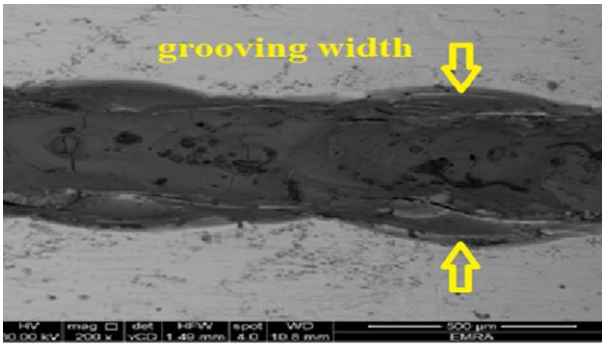

Fig. 15. SEM micrograph of (LTP) for armored steel (500HB) assisted by oxygen at multi-optimal parametric setting for maximize MRR, UC, LC, DC and minimize RE

6. Confirmation experiments

In order to validate the optimal results that are obtained by the composite desirability optimization technique, the obtained operating conditions are adopted for conducting an experimental trial. The five responses were measured for the confirmation trail, as listed by table 12. After comparing the obtained actual results with the optimal expected results the errors were computed. The errors between expected values and real values for MRR, RE, DC, UC and LC lie between 2.8%, 2.6%, 2.9%, 1% and 6.9% successively. Clearly, the later errors prove very good reproductively of the trialing results. The SEM view of CO_2 laser turning process (LTP) for armored steel (500HB) assisted by oxygen at optimum parametric combination is shown in figure. 15.

7. Conclusions

This paper investigates the behavior of grooving Armor steel using CO_2 laser turning process assisted by Oxygen. Four operating parameters were used as process controllers which include Laser power, pressure of the assisted gas, feed rate, and the motor speed. Five performance metrics were adopted for grooving of Armor steel that include Metal removal rate (MRR), roundness error (RE), groove's depth of cut (DC), upper cut (UC), and lower cut (LC). The process was analyzed using response surface methodology (RSM). The mathematical model of each response was developed with satisfactory very high coefficients of determinates and ANOVA results. The obtained R^2 is about 0.925, 0.935, 0.91, and 0.90 for each of MRR, RE, DC, UC, and R^2 is about 0.92 for LC. The adequacy of using CO_2 Laser turning was proven for turning armor steel with acceptable responses. For MRR and RE, feed rate is the most important controller, then come the other parameters. For the DC of the groove, laser power is the principle controller, then come the other parameters. For groove's UC, motor speed was found as the most important controller then comes the laser power. For groove's LC, laser power was found as the most important controller then comes the assessed gas pressure. Relying on the developed mathematical model of each response the composite desirability function was used for performing the multi-response optimization. The optimal settings are obtained as Laser power= 1934.944 watt, O_2 gas pressure= 0.60 bar, feed rate = 308.85 mm/min and motor speed rate = 26.566 r.p.m for obtaining the best compromising amongst MRR, RE, DC, UC, and LC. After implementing the optimal operating conditions experimentally, the real performance values were measured and compared with the analytical results. The error between the analytical and real performance values for MRR, RE, DC, UC and LC lie between 2.8%, 2.6%, 2.9%, 1% and 6.9% respectively. This investigation will open up furthermore scope to investigate the machined surface integrity, other turning processes, other alloys and other assisted gases for utilizing CO_2 laser turning process more effectively.

8. Acknowledgments

The authors acknowledge the helping provided by Eng. Abdel Sadek Ahmed, chairman of (Kader Factory for Developed Industries), A.O.I, Nasr city, Arab republic of Egypt, for his assistance in the experimental work performed on CO_2 laser cutting m/c.

9. Abbreviations:

RSM	Response surface methodology
LTMP	Laser turning machining process
ANO	Analysis of variance
ṀRR	Metal removal rate
DC	Depth of cut
UC	Upper cut
LC	Lower cut
RE	Roundness error
LBM	Laser beam machining
D	Composite desirability
di	Desirability for ith response
Hi	Highest acceptable value for ith response
i	Predicted value of ith response;
Li	Lowest acceptable value for ith response
n	Number of responses
ri	Weight of desirability function of ith response
Ti	Target value for ith response
wi	Importance of ith response
ε	Fitting error of the uth observations
SR	Surface Roughness

References:

[1] G. Chryssolouris, Laser machining: theory and practice, Springer, NewYork, 2013.

[2] J.F. Ready, D.F. Farson, T. Feeley, eds., LIA Handbook of Laser Materials Processing, Springer-Verlag, Berlin Heidelberg, 2001. https://www.springer.com/gp/book/9783540417705 (accessed July 13, 2020).

[3] H.J. Booth, Recent applications of pulsed lasers in advanced materials processing, Thin Solid Films. 453–454 (2004) 450–457. https://doi.org/10.1016/j.tsf.2003.11.130.

[4] A.S. Kuar, B. Doloi, B. Bhattacharyya, Modelling and analysis of pulsed Nd:YAG laser machining characteristics during micro-drilling of zirconia (ZrO_2), International Journal of Machine Tools and Manufacture. 46 (2006) 1301–1310.

https://doi.org/10.1016/j.ijmachtools.2005.10.016.

[5] D. Engin, K.W. Kirby, Development of an analytical model for the laser machining of ceramic and glass- ceramic materials, Journal of Applied Physics. 80 (1996) 681–690. https://doi.org/10.1063/1.362877.

[6] K. Farooq, A. Kar, Removal of laser-melted material with an assist gas, Journal of Applied Physics. 83 (1998) 7467–7473. https://doi.org/10.1063/1.367509.

[7] C.-C. Mai, J. Lin, Supersonic flow characteristics in laser grooving, Optics & Laser Technology. 35 (2003) 597–604. https://doi.org/10.1016/S0030-3992(03)00083-5.

[8] H.A.G. El-Hofy, Advanced machining processes: Nontraditional and hybrid machining processes, McGraw Hill Professional., 2005.

[9] J.P. Davim, N. Barricas, M. Conceição, C. Oliveira, Some experimental studies on CO_2 laser cutting quality of polymeric materials, Journal of Materials Processing Technology. 198 (2008) 99–104. https://doi.org/10.1016/j.jmatprotec.2007.06.056.

[10] E. Nagels, J.R. Duflou, J. Van Humbeeck, The influence of sulphur content on the quality of laser cutting of steel, Journal of Materials Processing Technology. 194 (2007) 159–162. https://doi.org/10.1016/j.jmatprotec.2007.04.103.

[11] J. De Keuster, J.R. Duflou, J.-P. Kruth, Monitoring of high-power CO_2 laser cutting by means of an acoustic microphone and photodiodes, Int J Adv Manuf Technol. 35 (2007) 115–126. https://doi.org/10.1007/s00170-006-0695-z.

[12] C.Y. Ho, M.Y. Wen, J.E. Ho, D.Y. Chen, Temperature history for cutting of ceramics preheated by a CO_2 laser, Journal of Materials Processing Technology. 192–193 (2007) 525–531. https://doi.org/10.1016/j.jmatprotec.2007.04.017.

[13] B.S. Yilbas, A.F.M. Arif, C. Karatas, M. Ahsan, Cemented carbide cutting tool: Laser processing and thermal stress analysis, Applied Surface Science. 253 (2007) 5544–5552. https://doi.org/10.1016/j.apsusc.2006.12.123.

[14] C.-H. Tsai, B.-C. Lin, Laser cutting with controlled fracture and pre-bending applied to LCD glass separation, Int J Adv Manuf Technol. 32 (2007) 1155–1162. https://doi.org/10.1007/s00170-006-0422-9.

[15] A. Parthiban, T. Sathish, S.S. Chandran, R. Venkatesh, V. Vijayan, Optimization of CO_2 laser cutting parameters on austenite stainless steel using grey relational analysis, International Journal of Mechanical Engineering and Technology. 10 (2019) 984–992.

[16] B. El Aoud, M. Boujelbene, E. Bayraktar, S. Ben Salem, I. Miskioglu, Studying Effect of CO_2 Laser Cutting Parameters of Titanium Alloy on Heat Affected Zone and Kerf Width Using the Taguchi Method, in: P.R. Thakre, R. Singh, G. Slipher (Eds.), Mechanics of Composite and Multi-Functional Materials, Volume 6, Springer International Publishing, Cham, 2018: pp. 143–150. https://doi.org/10.1007/978-3-319-63408-1_14.

[17] A. Alizadeh, H. Omrani, An integrated multi response Taguchi- neural network- robust data envelopment analysis model for CO_2 laser cutting, Measurement. 131 (2019) 69–78. https://doi.org/10.1016/j.measurement.2018.08.054.

[18] M. Madić, S. Mladenović, M. Gostimirović, M. Radovanović, P. Janković, Laser cutting optimization model with constraints: Maximization of material removal rate in CO_2 laser cutting of mild steel, Proceedings of the Institution of Mechanical Engineers, Part B: Journal of Engineering Manufacture. 234 (2020) 1323–1332. https://doi.org/10.1177/0954405420911529.

[19] D. Kumar, S. Gururaja, Investigation of hole quality in drilled Ti/CFRP/Ti laminates using CO_2 laser, Optics & Laser Technology. 126 (2020) 106130. https://doi.org/10.1016/j.optlastec.2020.106130.

[20] M. Khajehzadeh, M.R. Razfar, Process parameters influence on laser-assisted machining-induced residual stresses, Materials and Manufacturing Processes. 0 (2020) null. https://doi.org/10.1080/10426914.2020.1784930.

[21] P.K. Shrivastava, B. Singh, Y. Shrivastava, A.K. Pandey, D. Nandan, Investigation of optimal process parameters for laser cutting of Inconel-718 sheet, Proceedings of the Institution of Mechanical Engineers, Part C: Journal of Mechanical Engineering Science. 234 (2020) 1581–1597. https://doi.org/10.1177/0954406219895533.

[22] C. Zhai, J. Xu, Y. Li, Y. Hou, S. Yuan, Q. Liu, X. Wang, The Study on Surface Integrity on Laser-assisted Turning of SiC_p/2024Al, in: 2019 IEEE International Conference on Manipulation, Manufacturing and Measurement on the Nanoscale (3M-NANO), 2019: pp. 1–6. https://doi.org/10.1109/3MNANO46308.2019.8947388.

[23] J. Mesicek, J. Petru, T. Zlamal, M. Pagac, J. Sedivy, O. Vortel, L. Drabek, The Use of Technology Local Heating by Laser for Turning of Difficult to Machine Materials, in: S. Hloch, D. Klichová, G.M. Krolczyk, S. Chattopadhyaya, L. Ruppenthalová (Eds.), Advances in Manufacturing Engineering and Materials, Springer International Publishing, Cham, 2019: pp. 290–298. https://doi.org/10.1007/978-3-319-99353-9_31.

[24] T. Kim, K.-K. Kwon, C.N. Chu, K.Y. Song, Experimental investigation on CO_2 laser-assisted micro-slot milling characteristics of borosilicate glass, Precision Engineering. 63 (2020) 137–147. https://doi.org/10.1016/j.precisioneng.2020.02.004.

[25] Ammar H. Elsheikh, wu Deng, Ezzat A. Showaib, Improving laser cutting quality of polymethylmethacrylate sheet: experimental investigation and optimization, Journal of Materials Research and Technology. 9 (2020) 1325–1339. https://doi.org/10.1016/j.jmrt.2019.11.059.

[26] E. Haddadi, M. Moradi, A. Karimzad Ghavidel, A. Karimzad Ghavidel, S. Meiabadi, Experimental and parametric evaluation of cut quality characteristics in CO_2 laser cutting of polystyrene, Optik. 184 (2019) 103–114. https://doi.org/10.1016/j.ijleo.2019.03.040.

[27] D.C. Montgomery, Design and analysis of experiments, John Wiley, New York., 2001.

[28] U. Çaydaş, A. Hasçalık, Use of the grey relational analysis to determine optimum laser cutting parameters with multi-performance characteristics, Optics & Laser Technology. 40 (2008) 987–994. https://doi.org/10.1016/j.optlastec.2008.01.004.

[29] G. Derringer, R. Suich, Simultaneous Optimization of Several Response Variables, Journal of Quality Technology. 12 (1980) 214–219. https://doi.org/10.1080/00224065.1980.11980968.

[30] T.A. El-Taweel, Multi-response optimization of EDM with Al–Cu–Si–TiC P/M composite electrode, Int J Adv Manuf Technol. 44 (2009) 100–113.https://doi.org/10.1007/s00170-008-1825-6.

[31] D. Dhupal, B. Doloi, B. Bhattacharyya, Pulsed Nd:YAG laser turning of micro-groove on aluminum oxide ceramic (Al_2O_3), International Journal of Machine Tools and Manufacture. 48 (2008) 236–248. https://doi.org/10.1016/j.ijmachtools.2007.08.016 .

[32] G. Kibria, B. Doloi, B. Bhattacharyya, Predictive model and process parameters optimization of Nd:YAG laser micro-turning of ceramics, Int J Adv Manuf Technol (2013).

[33] R. Adalarasan, M. Santhanakumar, S. Thileepan, Selection of optimal machining parameters in pulsed CO_2 laser cutting of Al6061/Al_2O_3 composite using Taguchi-based response surface methodology (T-RSM), Int J Adv Manuf Technol 93:305–317(2017).

[34] D. Kondayya, A. Gopala Krishna, An integrated evolutionary approach for modeling and optimization of laser beam cutting process, International Journal of Advanced Manufacturing Technology, 65 (1) 259-274, (2013).

[35] A. Tamilarasan, D. Rajamani, Multi-response optimization of Nd: YAG laser cutting parameters of Ti-6Al- 4V super alloy sheet, Journal of Mechanical Science and Technology 31 (2) (2017) 813~821. www.springerlink.com/content/1738-494x (Print)/1976-3824(Online), DOI10.1007/s12206-017-0133-1

[36] Muneer Khan Mohammed, Abdulrahman Al-Ahmari, Multi-response optimization of machining parameters in micro milling of alumina ceramics using Nd: YAG laser Usama Umer, Measurement 95 (2017) 1891-192.

[37] G. Kibria , B. Doloi, B. Bhattacharyya, Experimental investigation and multi-objective optimization of Nd:YAG laser micro-turning process of alumina ceramic using orthogonal array and grey relational analysis, Optics& laser technology 48 (2013) 16-27.

[38] R. Biswas, A.S. Kuar, S. Mitra, " Multi-objective optimization of hole characteristics during pulsed Nd: YAG laser micro drilling of gamma-titanium aluminide alloy sheet " Optics and Lasers in Engineering, vol.60, pp 1-11, 2014.

[39] Yayun Liu, Lili Liu, Jianxin Deng, Rong Meng, Xueqian Zou, Fengfang Wu, " Fabrication of micro-scale textured grooves on green ZrO_2 ceramics by pulsed laser ablation", Ceramics International, vol 43, pp 6519-6531,2017.